Degrees of freedom and the dynamics of fully developed turbulence

Diego Donzis * and Shilpa Sajeev
Department of Aerospace Engineering, Texas A&M University, College Station, Texas 77843, USA

(Received 11 July 2023; accepted 15 March 2024; published 15 April 2024; corrected 8 July 2024)

While the degrees of freedom needed to represent the dynamics of high Reynolds number turbulence are extremely large, we show using well-resolved direct numerical simulations that one can capture essential physics with only a fraction of modes obeying the Navier-Stokes equations; the other modes can be modeled with very simple dynamics. This result suggests that the attractor for the dynamics of fully developed turbulence is robust to modeling errors and the strongly nonlinear dynamics may reside on fewer degrees of freedom than traditionally thought. The proposed approach is validated in terms of dissipation rate, skewness of velocity gradients, the energy and transfer spectrum, and structure functions. The mixed-dynamics model explored here, which may open different venues for turbulence modeling, may also be applicable to a broader set of physical phenomena governed by nonlinear complex dynamics with a wide range of scales.

DOI: 10.1103/PhysRevFluids.9.044605

I. INTRODUCTION

A distinguishing feature of turbulent flows is their wide range of spatial and temporal scales present at high Reynolds numbers typically found in natural flows and man-made systems. These scales, commonly represented by Fourier modes, interact nonlinearly producing energy transfers from the largest scales where turbulence production typically dominates and most of the energy resides, to the smallest scales where viscous effects dominate and dissipation converts turbulent kinetic energy into internal energy. This leads to the important question of determining the number of degrees of freedom needed to represent accurately the dynamics of the system. The classical phenomenology of Kolmogorov [1] posits that the ratio of the integral (or correlation) length scale (L) to the smallest dynamically relevant scales (η, the Kolmogorov scale) is $L/\eta \sim R_\lambda^{3/2}$ where R_λ is the Reynolds number based on the Taylor microscale. The number of modes needed to represent the physics faithfully in three dimensions is then $N^3 \sim (L/\eta)^3 \sim R_\lambda^\alpha$ where $\alpha = 9/2$. This steep power law illustrates the enormous range of modes needed at high R_λ which leads to tremendous difficulties to understand, model, and simulate these flows. Other estimates of the degrees of freedom have been made in the literature to account for the so-called intermittency phenomenon, leading to even steeper exponents: $\alpha = 6/(1 + h_{\min})$ where $h_{\min}$ is the smallest local exponent for velocity differences [2], $\alpha = 12/(s + 1)$ where s is the spectral slope [3], $\alpha = 5.4$ [4], or $\alpha = 6$ [5]. As pointed out in Ref. [3], though, most estimates are an upper bound to the degrees of freedoms needed for a general solution to the Navier-Stokes equations, noting that some flows may in fact need fewer modes. This issue is also important in a broader context since the main challenge in simulating atmospheric or astrophysical flows is the massive computational cost incurred in evolving a dynamical system with an exceedingly large range of nonlinearly interacting scales in a very large attractor. Identifying a smaller set of modes which contains some of the essential dynamics of turbulent flows not only will

*donzis@tamu.edu

provide a framework to devise less costly computational approaches for these flows but also may provide a simpler dynamical system over which the fundamental features of turbulent flows may be more readily understood.

In this paper, we show that one can indeed represent the dynamics of turbulence accurately by evolving only a subset of modes according to the Navier-Stokes equations at a time. The rest can be modeled with trivially simple dynamics.

The main idea is to evolve a subset of scales according to Navier-Stokes dynamics (the *resolved* modes), but unlike decimation approaches [6], we do not discard modes. Instead, these *unresolved* modes are evolved using simple dynamics. Thus, while only a fraction of modes is evolved according to Navier-Stokes dynamics at an instant of time, over time all modes will obey (at different instants) the exact governing equations. The subset of unresolved modes is chosen randomly at each step in the integration procedure. This ensures that all modes will follow Navier-Stokes dynamics at rates that, as we show, can be changed to capture accurately the different processes. Because a subset of modes is selected to be resolved at each step, in what follows, this approach will be called selected-eddy simulations or SES for short, to distinguish it from direct numerical simulations (DNS).

In a periodic domain, we can formally introduce this approach by splitting the Fourier representation of the velocity field into resolved (subscript r) and unresolved (subscript u) modes,

$$\boldsymbol{u}(\boldsymbol{x}) = \sum_{\boldsymbol{k}\in\boldsymbol{k}_r} \hat{\boldsymbol{u}}(\boldsymbol{k}) e^{\iota \boldsymbol{x}\cdot\boldsymbol{k}} + \sum_{\boldsymbol{k}\in\boldsymbol{k}_u} \hat{\boldsymbol{u}}(\boldsymbol{k}) e^{\iota \boldsymbol{x}\cdot\boldsymbol{k}}, \tag{1}$$

or simply $\boldsymbol{u}(\boldsymbol{x}) = \boldsymbol{u}_r(\boldsymbol{x}) + \boldsymbol{u}_u(\boldsymbol{x})$. Here, $\iota = \sqrt{-1}$, $\hat{\boldsymbol{u}}(\boldsymbol{k})$ is the Fourier mode at wave number $\boldsymbol{k}$, and $\boldsymbol{k}_r$ and $\boldsymbol{k}_u$ are the set of wave numbers corresponding to resolved and unresolved modes, respectively. Note that $\boldsymbol{k}_r \cap \boldsymbol{k}_u = \emptyset$. The cardinality of $\boldsymbol{k}_r$ and $\boldsymbol{k}_u$ will be denoted by $n(\boldsymbol{k}_r)$ and $n(\boldsymbol{k}_u)$, respectively. A simulation resolving all modes (that is, DNS) would then correspond to $n(\boldsymbol{k}_u) = 0$. Since the entire space is $\boldsymbol{k}_t = \boldsymbol{k}_r \cup \boldsymbol{k}_u$, we have $n(\boldsymbol{k}_t) = n(\boldsymbol{k}_u) + n(\boldsymbol{k}_r)$. We then define the fraction of resolved modes as $P_r \equiv n(\boldsymbol{k}_r)/n(\boldsymbol{k}_t)$.

The set $\boldsymbol{k}_r$ is selected randomly with a given probability, $p(k)$ which depends on the magnitude of the wave-number vector ($k = |\boldsymbol{k}|$). In other words, each scale of size $1/k$ in physical space is updated with Navier-Stokes dynamics with probability $p(k)$. Two distributions are used here: a uniform probability (denoted by U) with $p(k) = p_U$ where p_U is a constant, and a variable distribution (V for short) where $p(k) = \exp(-p_V k)$ with p_V being a constant. The rationale for the latter distribution is that a U distribution selects more Navier-Stokes dynamics at high wave numbers since the number of modes with $|\boldsymbol{k}| = k$ grows as k^2 (area of a sphere in Fourier space). The exponentially decaying $p(k)$ provides a comparison case where more (less) modes are resolved at low (high) wave numbers than the U distribution.

The unresolved modes are modeled here using a zeroth-order extrapolation in time which, by virtue of being the simplest model, may provide insight on how crudely one can model the dynamics at different scales and still capture the essential features of the flow.

Formally, the Navier-Stokes equations in Fourier space can be written symbolically as

$$d\hat{\boldsymbol{u}}(\boldsymbol{k})/dt = \mathcal{L}(\hat{\boldsymbol{u}}), \tag{2}$$

where

$$\mathcal{L}(\hat{\boldsymbol{u}}) = -ik_l P_{im} \int_{\boldsymbol{k}'} \hat{u}_m(\boldsymbol{k}')\hat{u}_l(\boldsymbol{k}-\boldsymbol{k}')d\boldsymbol{k}' - \nu k^2 \hat{u}_i(\boldsymbol{k}), \tag{3}$$

with the projection tensor defined as $P_{im} = \delta_{im} - k_i k_m/k^2$ and ν being the viscosity. In discretized form, SES can then be succinctly written as

$$\hat{\boldsymbol{u}}_{n+1}(\boldsymbol{k}) = \begin{cases} \hat{\boldsymbol{u}}_n(\boldsymbol{k}) + \Delta t\, \mathcal{L}(\hat{\boldsymbol{u}}_n) & \text{if } \gamma(\boldsymbol{k}) \leqslant p(k), \\ \hat{\boldsymbol{u}}_n(\boldsymbol{k}) & \text{otherwise,} \end{cases} \tag{4}$$

TABLE I. Simulation parameters: $R_\lambda = u'\lambda/\nu$ is the Taylor Reynolds number (λ and ν are Taylor scale and viscosity, respectively), $P_r = n(\boldsymbol{k}_r)/n(\boldsymbol{k}_t)$ is the percentage of resolved modes, and N^3 is the grid resolution.

R_λ range	P_r	N
40–42	U: 0.1, 0.22, 0.44, 0.62, 0.78, 0.93	64
28–42	V: 0.1, 0.22, 0.44, 0.62, 0.78, 0.93	
79–90	U: 0.1, 0.22, 0.44, 0.62, 0.78, 0.93	128
67–90	V: 0.1, 0.22, 0.44, 0.62, 0.78, 0.93	
126–143	U: 0.1, 0.22, 0.44, 0.62, 0.78, 0.93	256
90–143	V: 0.1, 0.22, 0.44, 0.62, 0.78, 0.93	
191–231	U: 0.1, 0.22, 0.44, 0.62, 0.78, 0.93	512
154–231	U: 0.1, 0.22, 0.44, 0.62, 0.78, 0.93	
299–376	U:0.1, 0.22, 0.44, 0.62, 0.78, 0.93	1024
196–376	U:0.1, 0.22, 0.44, 0.62, 0.78, 0.93	

where we use a simple one-step temporal discretization for the top equation for simplicity in the exposition. In this system, $\hat{\boldsymbol{u}}_n(\boldsymbol{k})$ is the velocity field at time step n, and γ is a uniformly distributed random number [$\gamma \sim U(0, 1)$] drawn for every wave number $\boldsymbol{k}$ at every step. In other words, the probability of a mode $\hat{\boldsymbol{u}}(\boldsymbol{k})$ to be evolved according to Navier-Stokes dynamics at a given time step is $p(k)$. The global fraction of resolved modes is then readily found to be $P_r = (3/k_{\max}^3)\int_0^{k_{\max}} p(k)k^2dk$ where $k_{\max}$ is the highest wave number resolved in the simulations. The simulations are based on the widely used pseudospectral approach of Ref. [7] with a second-order Runge-Kutta method for time integration. The time step size was determined from a Courant-Friedrichs-Lewy (CFL) number of 0.6 for all simulations, which has been shown to be adequate for the statistics shown here [8]. From Eq. (4), we can see that the difference between SES and DNS, i.e., the additional perturbation introduced at a single step by SES, goes to zero as $\Delta t \to 0$. A stationary state is maintained by applying a large-scale (or low-wave-number modes, with $k \lesssim 2$) random forcing based on independent integrated Ornstein-Uhlenbeck processes with a finite-time correlation, which balances the dissipative effects of viscosity at the smallest scales. This approach has been extensively used to study a wide range of aspects of turbulence [9–11]. The resolution for all cases satisfies $k_{\max}\eta \gtrsim 1.5$ which is enough to accurately resolve all dynamics of interest [9]. A summary of simulation parameters is shown in Table I. The range of Reynolds numbers in the first row indicates simulations with different P_r, with the lowest R_λ corresponding to the lowest P_r.

II. RESULTS

To assess the SES approach governed by the mixed-dynamics Eq. (4) we compare key variables characterizing turbulence dynamics with well-resolved DNS (i.e., $P_r = 1$) along with available results from the literature [12–22].

A basic result in turbulence is dissipative anomaly, as proposed by Taylor [23], which states that the rate at which turbulence dissipates fluctuating kinetic energy $\langle\epsilon\rangle \equiv \nu\langle \boldsymbol{s}^2\rangle$ becomes independent of viscosity as its value becomes small (or equivalently at high Reynolds numbers). A common way to assess this property is to plot the normalized dissipation rate $C_\epsilon \equiv \langle\epsilon\rangle L/u'^3$ where u' is the root mean square of a component of the velocity field, and observe an asymptote at high R_λ, i.e., $\lim_{R_\lambda\to\infty} C_\epsilon = C_{\epsilon,\infty}$. This property of turbulence, often known as the "zeroth law of turbulence," has been supported experimentally and numerically [17,24–41]. The basis for this result is that, while dissipation happens at the smallest scales where viscous effects are dominant, the rate at which this happens is set by the large scales. It is not surprising then that the observed value of $C_{\epsilon,\infty}$ depends on large-scale details of the flow or large-scale forcing used in numerical simulations [27]. This can be seen in Fig. 1 where we show the normalized dissipation rate which indeed tends to a constant at high R_λ though for different data sets the constant may be slightly different. For the

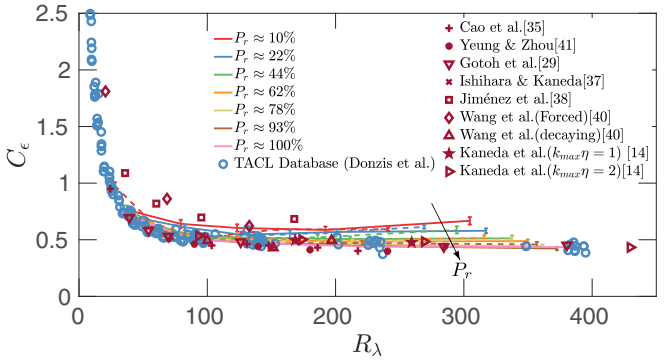

FIG. 1. Normalized dissipation rate $C_\epsilon = \langle\epsilon\rangle L/u'^3$. Lines correspond to U (dashed) and V (solid) distributions for different values of P_r in different colors. Symbols are for other DNS studies.

present results with $P_r < 1$ [i.e., $n(\boldsymbol{k}_u) > 0$] we can see that both U (dashed lines) and V (solid lines) distributions satisfy the dissipative anomaly even when the number of degrees of freedom following Navier-Stokes dynamics is as low as 10%. Differences with other simulation data are within the observed scatter.

The skewness of the velocity gradient $S = \langle(\partial_x u)^3\rangle/\langle(\partial_x u)^2\rangle^{3/2}$ is a measure of the nonlinearity of Navier-Stokes dynamics which leads to complex non-Gaussian behavior ($S = 0$ if Gaussian) beyond some critical Reynolds number [28]. It is also proportional to the rate of enstrophy production by vortex stretching. Its value is approximately constant at $S \approx -0.5$ though it may increase very slowly with Reynolds number at R_λ beyond $O(10^3)$ [19,29].

In Fig. 2 we see previous data along with the present simulations. Data from U distributions follow the expected constant value of -0.5 even for P_r as low as 10%. Data from V distributions, on the other hand, show increased departures from $S = -0.5$ as P_r decreases, an effect that is more pronounced at high R_λ. While still within the experimental scatter, there is a systematic trend with P_r for V distributions. This is expected given that U distributions inject more Navier-Stokes dynamics at high wave numbers, which is where most of the contribution to S comes from. Note that the lower value of $p(k)$ at high k for V distributions implies not only that there will be fewer resolved modes in that shell of radius k, but also that a particular mode in that shell will be resolved less frequently

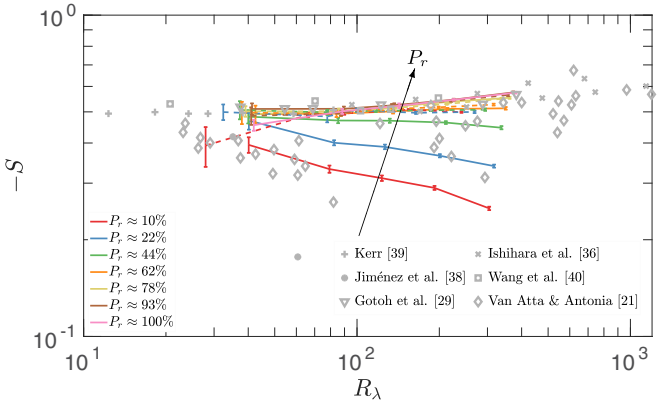

FIG. 2. Skewness of velocity gradients. Lines correspond to U (dashed) and V (solid) distributions for different values of P_r in different colors. Symbols except (◊) are for other DNS studies. The (◊) symbol corresponds to experimental data and are taken from Ref. [20].

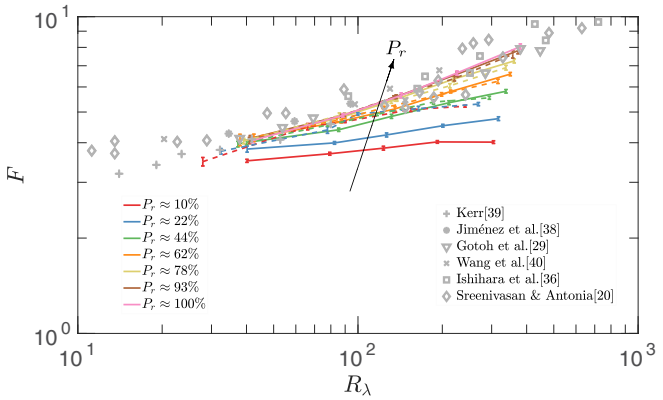

FIG. 3. Flatness of velocity gradients. Lines are for U (dashed) and V (solid) distributions. Symbols except (◊) are for other DNS studies. The (◊) symbol corresponds to experimental data and are taken from Ref. [19].

in time than another mode in a lower-k shell. We thus conclude that 10% of resolved modes seems sufficient for S as long as there is enough Navier-Stokes dynamics close to dissipative scales.

A similar observation can be made for the flatness of the velocity gradient $F = \langle(\partial_x u)^4\rangle/\langle(\partial_x u)^2\rangle^2$ which has also been extensively documented as a variable that can quantify the so-called intermittency (the tendency of turbulent flows to form extreme gradients which are localized in space and time [19]). A result of this phenomenon is the observed increase of F with the Reynolds number. This is seen in Fig. 3 where we show DNS and experimental data from the literature (gray symbols) along with results from U (dashed lines) and V (solid lines) distributions. As with the skewness, SES leads to results consistent with the literature even for very low values of P_r, especially for V distributions. It is interesting to note that SES does not lead to the almost-singular reduction of intermittency observed with decimation approaches where the removal of even a very small fraction of modes results in the virtual disappearance of intermittent behavior with approximately Gaussian statistics for high-order moments of velocity gradients and increments [30]. In contrast, we see in Fig. 3, a classical power-law increase of F with Reynolds numbers for V distributions even when only 10–20% of modes are resolved.

The energy spectrum is defined as $E(k) = (1/2)\int_{S(k)} |\hat{\boldsymbol{u}}(k)|^2 dS(k)$ where $S(k)$ is the surface on a shell of radius k in Fourier space, such that $\int_0^\infty E(k)dk$ is equal to the turbulent kinetic energy. In Fig. 4 we show the energy spectrum normalized according to Kolmogorov's similarity theory [1] for decreasing values of P_r for both U and V distributions (dashed and solid blue lines, respectively) along with a fully resolved DNS (solid red line). At $P_r \approx 78\%$ the spectrum for both U and V distributions follows closely the DNS spectrum which shows the classical Kolmogorov universality at small scales (collapse for all Reynolds numbers) with a bottleneck at $k\eta \approx 0.1$ and an inertial range ($1/L \ll k \ll 1/\eta$) with a Kolmogorov constant at $\approx$1.6 [10]. The lowest wave numbers, where forcing is applied ($k \lesssim 3$), are not expected to be universal and given their longer timescales, are more susceptible to stronger statistical variability which can explain the small variations across Reynolds numbers observed for the lowest wave numbers.

For U distributions (dashed blue lines) the dynamics at the smallest dissipative scales are accurately captured even at $P_r \approx 10\%$. At low wave numbers some differences with DNS are observed which are greater for U. This is not surprising given that V distributions contain more large-scale Navier-Stokes dynamics. However, for both cases, the general known features of the spectral distributions are clearly seen. Interestingly, all cases exhibit an inertial range seen as a plateau in Fig. 4 at intermediate wave numbers even when only 10% of modes are resolved in that range for the U case. The V case with $P_r \approx 10\%$, on the other hand, resolves 80%–90% of the modes in the inertial range, showing a weaker sensitivity to modeled dynamics than in other ranges

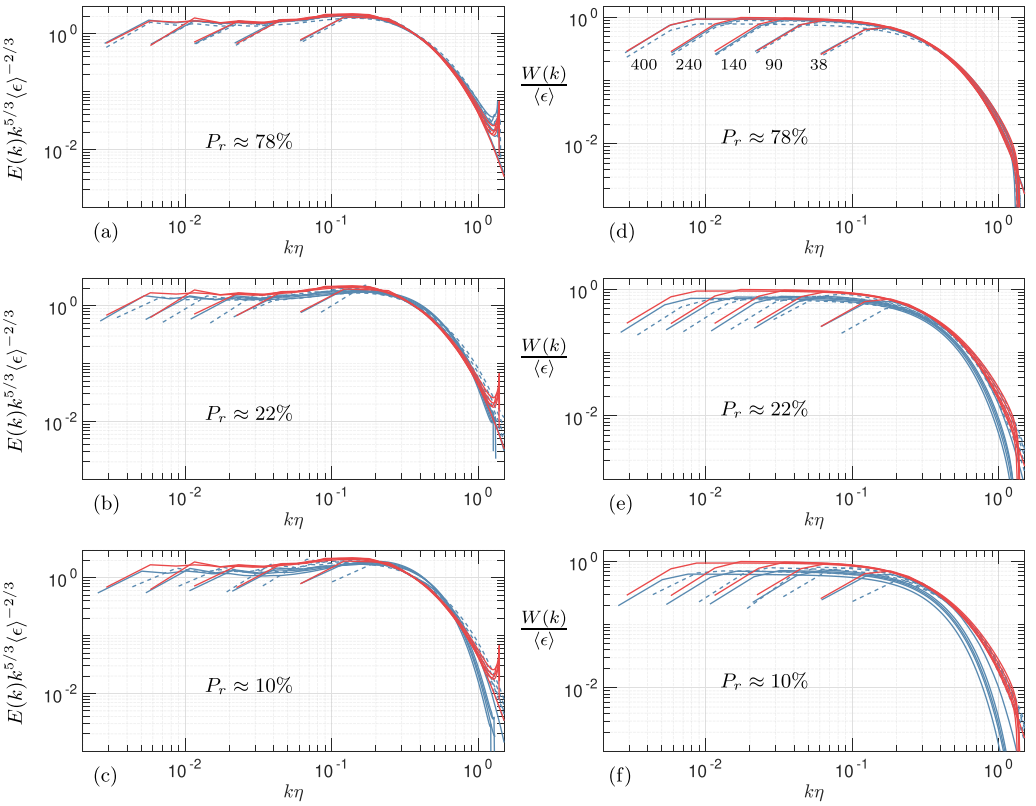

FIG. 4. Compensated energy spectrum [left panels, (a)–(c)] and transfer spectrum [right panels, (d)–(f)] vs $k\eta$ for different Reynolds numbers (indicated). Lines correspond to DNS (red solid), U distribution (blue dashed), and V distribution (blue solid).

of scales. For both cases we do observe a smaller Kolmogorov constant in the inertial range which, as we argue below, may be the result of a distributed forcing across all scales stemming from the mixed-dynamics model.

The total energy transfer through wave number k is given by $W(k) = \int_k^\infty T(k)dk$ where $T(k)$ is the dot product of $\hat{\boldsymbol{u}}(k)$ with the first term on the right-hand side of Eq. (3). In the inertial range, where both forcing and viscous effects are negligible, the energy transfer $W(k)$ is constant and equal to the rate of energy dissipation $\langle\epsilon\rangle$. This can be seen for the DNS data in Figs. 4(d)–4(f) where $W(k)/\langle\epsilon\rangle \approx 1$ in the inertial range. As P_r decreases though, this ratio decreases too, implying a transfer in the inertial range that is smaller than the rate at which energy is dissipated into heat at the small scales. These scales (beyond $k\eta \approx 0.1$ [10]) are better represented by a U distribution, not surprisingly given that it resolves more modes in the dissipative range.

Finally, in Fig. 5 we show the longitudinal structure functions $S_n(r) \equiv \langle[u(x+r) - u(x)]^n\rangle$ for $n = 2$, 3, and 4 from DNS (red lines) as well as SES (U distribution with blue dashed lines and V distributions with blue solid lines) with different probabilities P_r. The structure functions are compensated with $(\langle\epsilon\rangle r)^{n/3}$ to show an inertial range as a plateau. The third-order structure function, in particular, should plateau at 4/5 following Kolmogorov's 4/5th law (horizontal black line) at high enough Reynolds number. In Fig. 5(d) we indeed see $-S_3(r)/(\langle\epsilon\rangle r)$ from DNS approaching 4/5 in a manner completely consistent with the trends reported in the literature [31]. Results from SES with U and V distributions also exhibit a trend towards 4/5 albeit more slowly than DNS. Part of the reason for this behavior is that as P_r decreases, we observe a decrease in R_λ in the stationary state

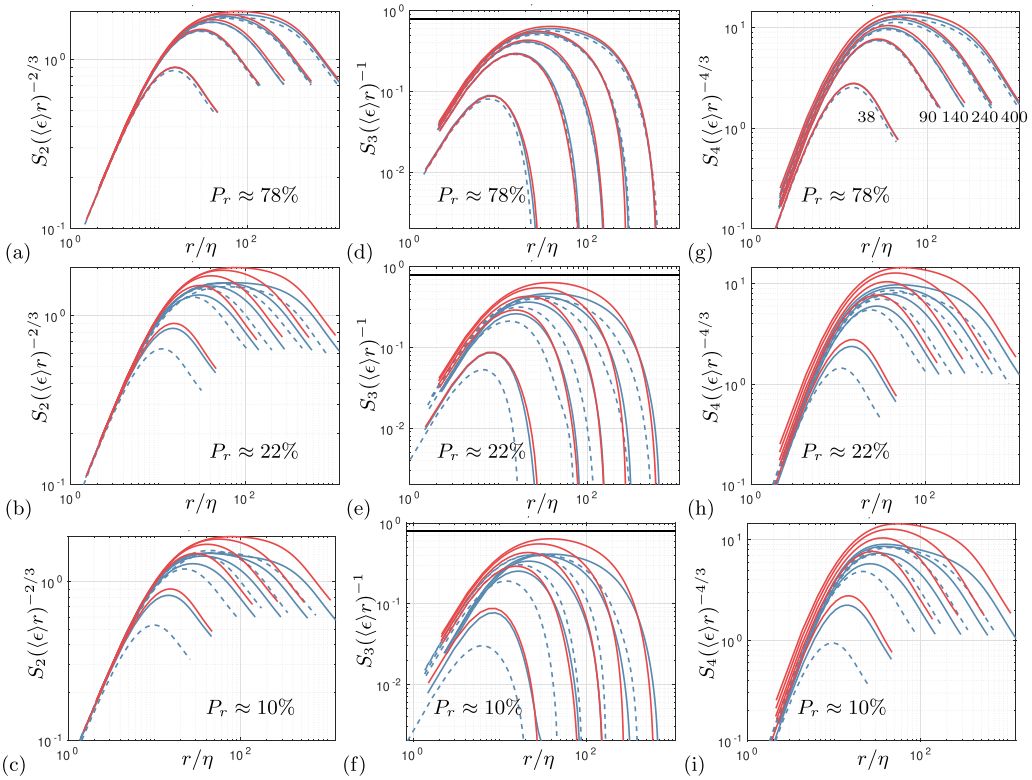

FIG. 5. Normalized longitudinal structure functions of order 2 (left), 3 (middle), and 4 (right) vs r/η for different Reynolds numbers (indicated). Lines correspond to DNS (red solid), U distribution (blue dashed), and V distribution (blue solid). The horizontal solid black line on the middle panels corresponds to $4/5$ for reference.

when all other parameters are fixed (see Table I). However, as discussed below, the main reason for this behavior is related to the mixed dynamics [Eq. (4)] whose effects can be cast as a distributed forcing which, as shown in the literature [32], leads to the differences seen in Figs. 5(d)–5(f). These trends are also observed for the second-order [Figs. 5(a)–5(c)] and fourth-order [Figs. 5(g)–5(i)] structure functions. From the latter, we again see that a rather large fraction of unresolved modes does not lead to the steep reduction of intermittency and consequent approach to Gaussian behavior for structure functions observed when modes are completely removed [30]. This observation suggest that while the overall number of modes that need to be included in the dynamics of the flow is similar to that required for DNS, in order to capture the intermittent structure of the small scales, only a fraction of them need to be evolved according to complex Navier-Stokes dynamics. The rest can be modeled using trivial dynamics. As with the spectra, structure functions exhibit greater departures from DNS at large scales for U distributions.

III. DISCUSSION

We have shown that important dynamical features of the Navier-Stokes solutions emerge even when only 10% of the modes traditionally thought to be critical to reproduce the behavior of high Reynolds number turbulence, are evolved using the exact governing equations. The rest of the modes, which are chosen randomly across wave numbers and time, can be easily modeled with simple dynamics. In this work, they were evolved according to a zeroth-order temporal extrapolation

as a worst case scenario. A further reduction in the percentage of resolved modes could be possible with the use of a higher-order temporal extrapolation. To quantify the gains this approach can attain, though, further studies will be needed.

A potential reason for the success of SES is that, unlike other widespread used approaches such as large-eddy simulations, the mixed-dynamics system proposed here allows for triadic interactions and transfers between all modes across the entire spectrum. It is well known [33–36] that distant transfers do occur though on average the cascade is in one direction (from large to small scales) and local (across scales of similar size). The availability of all modes (which is not the case for decimated approaches) allows for energy exchanges between all scales and thus more realistic dynamics.

Further, we can rewrite the Navier-Stokes equations in semidiscrete form (using a first-order discretization for simplicity, as before) as $\hat{\boldsymbol{u}}_{n+1} = \hat{\boldsymbol{u}}_n + \Delta t \mathcal{L}(\hat{\boldsymbol{u}})$. Now, when a mode is randomly selected to be modeled, we see that the last term in this expression vanishes according to Eq. (4). The result can then be written as $\hat{\boldsymbol{u}}_{n+1} = \hat{\boldsymbol{u}}_n + \Delta t \mathcal{L}(\hat{\boldsymbol{u}}) + F_{\text{SES}}$ where F_{SES} is an additional force that takes the specific form $-\Delta t \mathcal{L}(\hat{\boldsymbol{u}})$ leading to $\hat{\boldsymbol{u}}_{n+1} = \hat{\boldsymbol{u}}_n$. That is to say, the mixed-dynamics system can be thought of as the true Navier-Stokes equations with a random forcing distributed over modes across the entire spectrum. This observation allows us to explain the behavior of structure functions noted in the previous section. Lundgren [32] has shown that a distributed forcing produces structure functions that possess a much slower trend towards $4/5$ as the range of scales being forced increases. This is precisely what is observed in Fig. 5 for second- and third-order structure functions. The essence of the different approach towards the $4/5$ asymptote is the extra forcing term $\mathcal{I}$ in the Karman-Howarth equation [31]

$$S_3(r) = -\frac{4}{5}\langle\epsilon\rangle r + 6\nu\frac{\partial S_2(r)}{\partial r} + \mathcal{I}. \tag{5}$$

Here, $\mathcal{I}$ depends on the correlation between the velocity and forcing fields, i.e., $\langle \boldsymbol{u}(\boldsymbol{x}) \cdot \boldsymbol{F}(\boldsymbol{x}+\boldsymbol{r})\rangle$ and $\langle \boldsymbol{u}(\boldsymbol{x}+\boldsymbol{r}) \cdot \boldsymbol{F}(\boldsymbol{x})\rangle$. For a Gaussian forcing which is also delta correlated in time, for example, it is possible to obtain a closed form for $\mathcal{I}$ [13,37]. For SES, as argued above, the forcing mechanism will be comprised of two components, namely, the low-wave-number externally imposed stochastic driving force to keep turbulence in a statistical steady state, and the resulting forcing term stemming for the mixed dynamics of Eq. (4), F_{SES}. Regardless of the details of forcing, however, the important observation here is that even in the limit of vanishing viscosity, the term $\mathcal{I}$ does not vanish.

Further, in the case of forcing acting on all scales, one expects and indeed observes [31,38,39] flow- and forcing-dependent Reynolds number scaling as in Fig. 5. The general conclusion is thus that the SES approach introduced here can reproduce the physics at all scales while resolving only 10% of the modes according to Navier-Stokes dynamics with a distributed forcing. Note that this type of distributed forcing represents more closely the physics of flows with mean shear. This is so because in those flows, the production mechanism is proportional to the velocity field itself, that is, the forcing term is $S\hat{\boldsymbol{u}}$ (where S is the mean shear rate) and thus spans all scales. In classical phenomenology, at high enough Reynolds numbers, it is expected that turbulence would exhibit universal behavior regardless of forcing mechanism.

A related interesting observation is on the local effects of modeled modes. The skewness of velocity gradients, for example, is accurately computed when modeled modes cluster towards small scales (U distribution) which is expected given that the dominant contribution to gradients come from high wave numbers. However, dissipative anomaly seems to be largely unaffected by the distribution of modes. The implication seems to be that capturing local dynamics (in Fourier space) is important for the computation of statistics at those scales and less dependent on the dynamics at other scales. Because the frequency of updates is important at different scales, it will also be interesting to assess the effect of freezing a mode for multiple time steps (instead of a single step) or equivalently for a given time window. This would help inform appropriate switching schemes for Eq. (4) to capture accurately different processes with even smaller resolved modes.

We conclude by pointing out that the results presented here could also provide a venue for a computationally accessible approach to simulate other phenomena involving a massive range of

scales. The computational advantage of SES is severalfold. First, SES reduces the computational cost by reducing the number of modes that need to be advanced according to complex Navier-Stokes dynamics and replacing them by a much cheaper calculation based on a low-order temporal extrapolation. Second, in widely used pseudospectral implementations, transforms are completed as a series of one-dimensional fast Fourier transforms (FFTs) followed by transposes requiring collective communication across all processors. These communication operations, in fact, constitute the most expensive overhead associated with simulations at extreme levels of parallelism [40]. SES could potentially reduce significantly this cost by reducing the number of modes that need to be communicated at each time step. Finally, for very small values of P_r, it may be possible to take advantage of high-performance "pruned" FFTs [41]. These gains are important in a number of situations involving turbulent flows where critical processes appear at small scales (e.g., shock waves, reacting or weakly diffusive species) while turbulent production is mainly a large-scale nonuniversal phenomenon.

More broadly, our observations may be also applicable to other complex systems with large attractors and which may be accurately represented by sampling the attractor stochastically in phase space and time. The key in such a modeling effort would then revolve around understanding how to select and model those modes, and to what degree this approach can reduce the exponent α mentioned in the Introduction to obtain accurate simulations of all scales. The efforts here are a step in that direction.

ACKNOWLEDGMENT

The authors gratefully acknowledge support from the National Science Foundation (Grant No. 1605914) and from the Extreme Science and Engineering Discovery Environment (XSEDE) and the Texas Advanced Computing Center (TACC) for computational resources.

[1] A. N. Kolmogorov, Local structure of turbulence in an incompressible fluid for very large Reynolds numbers, Dokl. Akad. Nauk. SSSR **30**, 299 (1941).

[2] G. Paladin and A. Vulpiani, Degrees of freedom of turbulence, Phys. Rev. A **35**, 1971 (1987).

[3] P. Constantin, C. Foias, O. P. Manley, and R. Temam, Determining modes and fractal dimension of turbulent flows, J. Fluid Mech. **150**, 427 (1985).

[4] Z.-S. She and E. Leveque, Universal scaling laws in fully developed turbulence, Phys. Rev. Lett. **72**, 336 (1994).

[5] V. Yakhot and K. R. Sreenivasan, Anomalous scaling of structure functions and dynamic constraints on turbulence simulations, J. Stat. Phys. **121**, 823 (2005).

[6] U. Frisch, A. Pomyalov, I. Procaccia, and S. S. Ray, Turbulence in noninteger dimensions by fractal Fourier decimation, Phys. Rev. Lett. **108**, 074501 (2012).

[7] R. S. Rogallo, Numerical experiments in homogeneous turbulence, NASA Ames Research Center, Moffett Field, CA., NASA, NASA Tech. Memo. 81315, 1981.

[8] P. K. Yeung, K. R. Sreenivasan, and S. B. Pope, Effects of finite spatial and temporal resolution in direct numerical simulations of incompressible isotropic turbulence, Phys. Rev. Fluids **3**, 064603 (2018).

[9] D. A. Donzis, P. K. Yeung, and K. R. Sreenivasan, Dissipation and enstrophy in isotropic turbulence: Scaling and resolution effects in direct numerical simulations, Phys. Fluids **20**, 045108 (2008).

[10] D. A. Donzis and K. R. Sreenivasan, The bottleneck effect and the Kolmogorov constant in isotropic turbulence, J. Fluid Mech. **657**, 171 (2010).

[11] P. K. Yeung, D. A. Donzis, and K. R. Sreenivasan, High-Reynolds-number simulation of turbulent mixing, Phys. Fluids **17**, 081703 (2005).

[12] N. Cao, S. Chen, and G. D. Doolen, Statistics and structures of pressure in isotropic turbulence, Phys. Fluids **11**, 2235 (1999).

[13] G. Gotoh, D. Fukayama, and T. Nakano, Velocity field statistics in homogeneous steady turbulence obtained using a high-resolution direct numerical simulation, Phys. Fluids **14**, 1065 (2002).
[14] T. Ishihara, Y. Kaneda, M. Yokokawa, K. Itakura, and A. Uno, Small-scale statistics in high-resolution direct numerical simulation of turbulence: Reynolds number dependence of one-point velocity gradient statistics, J. Fluid Mech. **592**, 335 (2007)
[15] T. Ishihara and Y. Kaneda, High Resolution DNS of incompressible homogeneous forced turbulence—Time dependence of the statistics, *in Statistical Theories and Computational Approaches to Turbulence*, edited by Y. Kaneda and T. Gotoh (Springer Japan, Tokyo, 2003), pp. 177–188.
[16] J. Jiménez, A. A. Wray, P. G. Saffman, and R. S. Rogallo, The structure of intense vorticity in isotropic turbulence, J. Fluid Mech. **255**, 65 (1993).
[17] Y. Kaneda, T. Ishihara, M. Yokokawa, K. Itakura, and A. Uno, Energy dissipation rate and energy spectrum in high resolution direct numerical simulations of turbulence in a periodic box, Phys. Fluids **15**, L21 (2003).
[18] R. M. Kerr, Higher-order derivative correlations and the alignment of small-scale structures in isotropic numerical turbulence, J. Fluid Mech. **153**, 31 (1985).
[19] K. R. Sreenivasan and R. A. Antonia, The phenomenology of small-scale turbulence, Annu. Rev. Fluid Mech. **29**, 435 (1997).
[20] C. W. Van Atta and R. A. Antonia, Reynolds number dependence of skewness and flatness factors of turbulent velocity derivatives, Phys. Fluids **23**, 252 (1980).
[21] L. P. Wang, S. Chen, J. G. Brasseur, and J. C. Wyngaard, Examination of hypotheses in the Kolmogorov refined turbulence theory through high-resolution simulations. Part 1. Velocity field, J. Fluid Mech. **309**, 113 (1996).
[22] P. K. Yeung and Y. Zhou, Universality of the Kolmogorov constant in numerical simulations of turbulence, Phys. Rev. E **56**, 1746 (1997).
[23] G. I. Taylor, Statistical theory of turbulence, Proc. R. Soc. London, Ser. A **151**, 421 (1935).
[24] D. A. Donzis, K. R. Sreenivasan, and P. K. Yeung, Scalar dissipation rate and dissipative anomaly in isotropic turbulence, J. Fluid Mech. **532**, 199 (1999).
[25] K. R. Sreenivasan, On the scaling of the turbulence energy-dissipation rate, Phys. Fluids **27**, 1048 (1984).
[26] K. R. Sreenivasan, An update on the energy dissipation rate in isotropic turbulence, Phys. Fluids **10**, 528 (1998).
[27] C. R. Doering and C. Foias, Energy dissipation in body-forced turbulence, J. Fluid Mech. **467**, 289 (2002).
[28] V. Yakhot and D. A. Donzis, Emergence of multiscaling in a random-force stirred fluid, Phys. Rev. Lett. **119**, 044501 (2017).
[29] T. Ishihara, T. Gotoh, and Y. Kaneda, Study of high-Reynolds number isotropic turbulence by direct numerical simulation, Annu. Rev. Fluid Mech. **41**, 165 (2009).
[30] A. S. Lanotte, R. Benzi, S. K. Malapaka, F. Toschi, and L. Biferale, Turbulence on a fractal Fourier set, Phys. Rev. Lett. **115**, 264502 (2015).
[31] R. A. Antonia and P. Burattini, Approach to the 4/5 law in homogeneous isotropic turbulence, J. Fluid Mech. **550**, 175 (2006).
[32] T. S. Lundgren, Linearly forced isotropic turbulence, *Annual Research Briefs* (Center for Turbulence Research, Stanford, CA, 2003), pp. 461–473.
[33] J. A. Domaradzki, Analysis of energy-transfer in direct numerical simulations of isotropic turbulence, Phys. Fluids **31**, 2747 (1988).
[34] J. A. Domaradzki and D. Carati, An analysis of the energy transfer and the locality of nonlinear interactions in turbulence, Phys. Fluids **19**, 085112 (2007).
[35] P. K. Yeung and J. G. Brasseur, The response of isotropic turbulence to isotropic and anisotropic forcing at the large scales, Phys. Fluids **3**, 884 (1991).
[36] P. K. Yeung, J. G. Brasseur, and Q. Z. Wang, Dynamics of direct large-small scale couplings in coherently forced turbulence - concurrent physical-space and Fourier-space views, J. Fluid Mech. **283**, 43 (1995).
[37] E. A. Novikov, Functionals and the random-force method in turbulence theory, Sov. Phys. JETP **20**, 1290 (1965).

[38] P. L. Carroll and G. Blanquart, The effect of velocity field forcing techniques on the Karman–Howarth equation, J. Turbul. **15**, 429 (2014).

[39] A. M. Sain and R. Pandit, Turbulence and multiscaling in the randomly forced navier-stokes equation, Phys. Rev. Lett. **81**, 4377 (1998).

[40] K. Ravikumar, D. Appelhans, and P. K. Yeung, GPU acceleration of extreme scale pseudo-spectral simulations of turbulence using asynchronism, *in Proceedings of the International Conference for High Performance Computing, Networking, Storage and Analysis, SC '19*, (Association for Computing Machinery, New York, 2019).

[41] F. Franchetti and M. Puschel, Generating high performance pruned FFT implementations, in *2009 IEEE International Conference on Acoustics, Speech and Signal Processing, Taipei, Taiwan* (IEEE, New York, 2009), pp. 549–552.

Correction: Several references in the reference list were numbered incorrectly and have now been renumbered to match the citations in text.